Carbohydrate Polymers 344 (2024) 122523

Contents lists available at ScienceDirect

Carbohydrate Polymers

journal homepage: www.elsevier.com/locate/carbpol

Stacking self-gluing cellulose II films: A facile strategy for the formation of novel all-cellulose laminates

Christina Dahlström [a,*], Ran Duan [a,b], Alireza Eivazi [a], Solange Magalhães [c], Luís Alves [c], Magnus Engholm [d], Ida Svanedal [a], Håkan Edlund [a], Bruno Medronho [a,e], Magnus Norgren [a]

[a] Surface and Colloid Engineering, FSCN Research Centre, Mid Sweden University, Holmgatan 10, SE-851 70 Sundsvall, Sweden
[b] Tetra Pak, Ruben Rausings gata, SE-221 00 Lund, Sweden
[c] University of Coimbra, CERES, Department of Chemical Engineering, 3030-790 Coimbra, Portugal
[d] Advanced Materials and Processes, FSCN Research Centre, Mid Sweden University, Holmgatan 10, SE-851 70 Sundsvall, Sweden
[e] MED—Mediterranean Institute for Agriculture, Environment and Development, CHANGE-Global Change and Sustainability Institute, Faculdade de Ciências e Tecnologia, Universidade do Algarve, Campus de Gambelas, Ed. 8, 8005-139 Faro, Portugal

ARTICLE INFO

Keywords:
All-cellulose laminates
LiOH/urea
Dissolution
Regeneration
Fibers

ABSTRACT

Cellulose laminates represent a remarkable convergence of natural materials and modern engineering, offering a wide range of versatile applications in sustainable packaging, construction, and advanced materials. In this study, novel all-cellulose laminates are developed using an environmentally friendly approach, where freshly regenerated cellulose II films are stacked without the need for solvents (for impregnation and/or partial dissolution), chemical modifications, or resins. The structural and mechanical properties of these all-cellulose laminates were thoroughly investigated. This simple and scalable procedure results in transparent laminates with exceptional mechanical properties comparable to or even superior to common plastics, with *E*-modulus higher than 9 GPa for a single layer and 7 GPa for the laminates. These laminates are malleable and can be easily patterned. Depending on the number of layers, they can be thin and flexible (with just one layer) or thick and rigid (with three layers). Laminates were also doped with 10 wt% undissolved fibers without compromising their characteristics. These innovative all-cellulose laminates present a robust, eco-friendly alternative to traditional synthetic materials, thus bridging the gap between environmental responsibility and high-performance functionality.

1. Introduction

Cellulose is a polysaccharide abundantly found in plant cell walls, widely renowned for its biodegradability, renewability, and non-toxicity (Klemm et al., 2005). It is the main compound lending structure and resilience in trees and plants. The rapidly increasing demand for goods circularly manufactured from renewable and sustainable sources has positioned cellulose in a prominent place. It is believed that polysaccharides, such as cellulose, can offer impactful solutions to many resource challenges of society and suppliers, thus contributing to the evolving demands of modern cultures and industries (Gericke et al., 2024).

In this context, composites solely based on cellulose, also known as "all-cellulose composites" (ACCs), have emerged as a groundbreaking class of materials, representing a promising innovation in the world of sustainable and environmentally responsible engineering (Baghaei & Skrifvars, 2020; Huber, Pang, et al., 2012; Tanpichai et al., 2022). ACCs have rapidly gained interest for potential applications in various fields, including their incorporation in building materials (e.g., insulation boards, acoustic panels, biodegradable composites); packaging (e.g., food and pharmaceutical packaging with superior barrier properties, strength, and sustainability); biomedical devices (e.g., scaffolds for tissue engineering, wound dressings, drug delivery systems, and implants due to their favorable biocompatibility, biodegradability, and structural properties); and different electronic systems (e.g., flexible electronics and sensor devices due to their unique electrical properties and mechanical features) (Baghaei & Skrifvars, 2020; Huber, Müssig, et al., 2012; Tanpichai et al., 2022). These ACCs can overcome the often-found poor fiber–matrix adhesion due to using materials of the same chemical composition. Hence, the mechanical properties of ACCs are found to

* Corresponding author.
E-mail address: christina.dahlstrom@miun.se (C. Dahlström).

https://doi.org/10.1016/j.carbpol.2024.122523
Received 9 February 2024; Received in revised form 17 July 2024; Accepted 18 July 2024
Available online 20 July 2024

exceed most conventional biobased-composites (Huber, Pang, et al., 2012) while remaining fully bio-based and biodegradable (Kalka et al., 2014). It should be noted that achieving high adhesion between natural fibers and a given polymeric matrix in a biocomposite is a demanding task, particularly for thermoplastic matrices. Often, such compatibility is enhanced through pre-treatment and modification of the fibers or via the addition of coupling agents.

Since cellulose cannot be melted, its processing often requires dissolution in a suitable solvent followed by regeneration in a "non-solvent" to form cellulose-based materials, such as fibers, particles, films, foams, aerogels, etc. (Lindman et al., 2015; Lindman et al., 2017, 2021; Medronho & Lindman, 2014, 2015). These dissolution and regeneration steps are particularly relevant for the preparation of ACC, where two main approaches have been suggested: 1) complete cellulose dissolution, followed by its regeneration in the presence of undissolved cellulose fibers; 2) partial dissolution and regeneration, i.e., the matrix phase is obtained in situ by regenerating the dissolved portion (Huber, Pang, et al., 2012). The former approach was pioneered by Nishino et al., who have suggested the complete dissolution of kraft fibers in the lithium chloride/dimethyl acetamide (LiCl/DMAc) solvent system followed by regeneration in the presence of ramie fibers, using methanol as the coagulation medium (Nishino et al., 2004; Soykeabkaew et al., 2009). The latter approach is exemplified, for instance, in the recent work by Baranov et al., where ACC laminates were formed via the partial dissolution of a woven textile of cellulose II using aqueous tetrabutylphosphonium hydroxide solutions (Baranov et al., 2021). The dissolved cellulose was then regenerated in ethanol to reform the cellulose II matrix phase in situ, which bonds the original undissolved textile fibers.

ACCs have rapidly gained recognition as competitive eco-friendly structural composites with improved mechanical features (Huber, Pang, et al., 2012). Nevertheless, it is striking that most developed ACCs are essentially thin films (<1 mm) and preferentially processed using the LiCl/DMAc solvent system. Other solvents have been considered for ACCs (i.e., NMMO, ionic liquids, etc.) (Huber, Pang, et al., 2012; Uusi-Tarkka et al., 2021). Of special interest is the use of NaOH-based solvent systems that are cost-effective and keep ACCs with lower environmental impact (Dormanns et al., 2016; Labidi et al., 2019; Qi et al., 2009; Uusi-Tarkka et al., 2022).

Successful attempts to produce thicker ACCs have been described, particularly by the Staiger group. For instance, a novel laminate approach focusing on the conventional hand lay-up method combined with the partial dissolution of 2D woven textiles composed of natural and man-made cellulose fibers was reported (Huber, Pang, et al., 2012). The layers were impregnated with an ionic liquid (1-butyl-3-methylimidazolium acetate) and heated under pressure (compression molding). As a result, the fiber surfaces partially dissolved, and after being compacted, a single ACC lamina was obtained. This process is highly inspired by the conventional approach of creating cellulose-based laminates, where multiple layers of paper or cellulose fabric are impregnated with thermosetting resins (i.e., phenolic, epoxy, melamine), binders, or other adhesive agents before curing under pressure and heat. Staiger's group has also reported another innovative method for the fabrication of ACC laminates coined as solvent infusion processing (SIP), which is based on a partial dissolution approach producing robust and thicker cellulose-based laminates (Dormanns et al., 2016). SIP is conceptually inspired by vacuum-assisted resin transfer molding (Williams et al., 1996).

It should be highlighted that in most of the approaches discussed above, the solvents used in ACCs or the binders, adhesives, and resins used in traditional laminates present environmental concerns. The use of friendlier processes is clearly a growing priority and, in this respect, Yang and Berglund have adopted water-based hot-pressing processing on degummed, alkali treated, aligned ramie fibers obtaining promising transparent all-cellulose films (Yang & Berglund, 2018). Similarly, Nilsson et al. reported a non-solvent process where all-cellulose I wood biocomposites were successfully compression molded from wet wood fibers (Nilsson et al., 2010). Song et al. have reported on the formation of densified wood laminates after hot-pressing delignified natural wood (Song et al., 2018), while Li et al. have developed friendly solvent-free ACCs laminates from stacking bacterial cellulose hydrogels (Li, Wang, et al., 2020). From a mechanistic viewpoint, due to the high hydrophilicity of cellulose molecules, a repulsive osmotic pressure is anticipated once the hydrated cellulose surfaces come into close contact during drying, which suggests that the hydrophobic interactions might not be the most relevant force for the laminate formation. The overall van der Waals interactions between cellulose surfaces is thus weakened under aqueous conditions (Notley et al., 2004). To reach close contact the so-called hydration layer must be removed, which might occur at elevated temperature.

The structural rearrangements of cellulose-cellulose interfaces have been investigated in situ during drying using micro-focusing grazing-incidence small-angle X-ray scattering and atomic force microscopy (Li et al., 2021). It was concluded that molecular interdiffusion, where cellulose molecular chains in the wet cellulose material will diffuse over the interphase, combined with structural rearrangement, including aggregation, increases the molecular contact area and thereby the adhesion between the two cellulose materials. These observations are intimately related to the so-called "hornification process", an inevitable phenomenon occurring when drying cellulosic fibers (Mo et al., 2022). Although the initial hornification mechanism primarily considered microscopic aspects, such as the increase in the degree of crosslinking within the fiber microstructure upon drying or water removal (Jayme & Hunger, 1956), molecular-scale phenomena, such as the irreversible (or partially irreversible) formation of irreversible hydrogen bonding and co-crystallization have also been suggested as part of the hornification process (Sjöstrand et al., 2023).

A recent study by Sellman et al., sheds light on the hornification phenomenon and provides further insight into the mechanisms involved in the formation of our laminates (Sellman et al., 2023). The authors suggest the use of CNF-based films as suitable systems for studying interfibrillar interactions associated with irreversible cellulose aggregation. They successfully relate the extent of hornification to the reswelling degree after heat treatment. Overall, the authors argue that the hornification phenomenon is kinetically limited: once water diffuses away during drying, and fibers come into close contact, the diffusion of water back into the cellulose network is a very slow process. The authors further add that the process is governed by non-covalent reversible interactions, such as the ones described above.

In the present work, we introduce novel ACC laminates formed by a simple, scalable, and environmentally friendly approach relying on the stacking of freshly regenerated cellulose II films without the need of any hazardus binders, adhesives or resins. The idea's uniqueness lies in using regenerated cellulose films and a simple modified drying process, which, to the best of our knowledge, has never been reported before. The careful drying of the self-adhesive layers sticks them together, ultimately forming a robust laminate without any matrix. No synthetic coatings, binding agents, or impregnation steps are required to ensure superior laminate robustness. Cellulose laminates could be sustainably developed to exhibit properties that are not only environmentally friendly, but also surpass those of traditional plastics in terms of competitiveness. Adding 10 wt% of fibers in some films with subsequent lamination gave equally good results. The all-cellulose laminates obtained were extensively characterized by different methodologies.

2. Material and methods

2.1. Chemicals

The cellulose used for dissolution/regeneration was a commercial dissolving pulp (α-cellulose content of 91 %) from Domsjö Fabriker Aditya Birla (Örnsköldsvik, Sweden). The weight-average molecular weight (M_w) was 3.21×10^5 g mol^{-1}, the intrinsic viscosity was 432 mL

g^{-1}, and the polydispersity index was 10.3, as determined by size-exclusion chromatography (MoRe Research AB, Sweden). The undissolved added fibers were bleached softwood kraft pulp (SCA Pure ECF 90) supplied by SCA, Östrand mill. Urea (≥99.5 %) was purchased from Sigma-Aldrich (Sweden), LiOH·H_2O (56.5 %) from Alfa Aesar (Germany), and ethanol (≥99.8 %) from VWR Chemicals (Sweden).

2.2. Cellulose dissolution

The cellulose pulp was dissolved following an adapted method (Cai & Zhang, 2005; Yang et al., 2019). In brief, 4 wt% of cellulose Domsjö pulp was added to a pre-cooled (−12 °C) aqueous solution of 4.6 wt% LiOH and 15 wt% urea, stirred at 1300 rpm for 2 min and frozen to −30 °C. The solid mixture was then thawed to −12 °C and stirred with a propeller at 1300 rpm for 2 min. The freeze-thawing-mixing process was repeated twice to ensure complete dissolution of the cellulose. The dope was further centrifugated with a JLA-16.250 fixed angle rotor (Beckman Coulter, USA) at 8000 rpm for 10 min to remove air bubbles. The final cellulose solution was clear, with no undissolved cellulose fibers (checked by visual inspection and polarized optical microscopy).

2.3. Preparation of cellulose single films and 3-layer laminates

The cellulose dopes were regenerated by casting the solution onto glass plates and immersed into an ethanol regeneration bath for 2 h. The films were then placed in a Milli-Q water bath to wash away the remaining LiOH and urea, and the water was changed daily for three days until a neutral pH was reached for the regenerated films. For the preparation of single layer samples, the thoroughly washed film was placed between two filter papers and two blotting papers on the outside and then dried in a Rapid Köthen (RK) (Frank-PTI GMBH, Germany) paper making system at 93 °C at −0.93 bar for ca. 20 min (transparent across the whole film). This film is named CL1. The same procedure was done for the fiber-containing films where 10 wt% undissolved fibers was added in the cellulose dope before film regeneration. This is conceptually similar procedure as described in the introduction section regarding the dissolution and regeneration method for the preparation of ACCs. The added amount of cellulose fibers (i.e., 10 wt%) was selected for comparison purposes, and thus it was not further optimized. The single layer film containing fibers is named CFL1.

In this work, laminates were formed with 3 layers. To do so, the procedure described above was repeated with three pieces of freshly thoroughly washed regenerated cellulose films, which were stacked together, placed between two filter papers and two blotting papers, and then dried in RK under vacuum until thoroughly dried (around 60 min, until transparent across the whole laminate). This sample is called CL3. 3-layer laminates containing 10 wt% undissolved fibers were also formed (named CFL3). Once the films were formed containing the undissolved fibers, they were stacked and dried as described above. The 3-layered fiber laminates were made using one fiber-containing film outwards on each side and one with no fibers in the middle to enhance the contact during lamination. The complete method for dissolving, regenerating, and forming the all-cellulose laminates is schematically represented in Fig. 1. The samples were kept sealed in airtight bags until further analysis. The potential transition from cellulose I to cellulose II, when the bleached kraft pulp fibers are mixed into the cellulose solution, was also evaluated. In brief, 5 g of the commercial kraft pulp sheet was added to a 300 g aqueous solution of 4.6 wt% LiOH and 15 wt% urea, and left to interact for 2 h. Upon contact with the LiOH/urea solvent, the fibers spontaneously dispersed. After 2 h, the fiber dispersion was dewatered by vacuum filtration using a Büchner funnel and a 120 mesh nylon filter. Similarly to the cast cellulose films, the dewatered fiber cake was placed in ethanol for 2 h, followed by washing in MilliQ-water (as described in Section 2.3) and drying for 30 min. Additionally, a reference sample was prepared by immersing 5 g of the kraft pulp sheet in 300 g of MilliQ-water for 12 min, followed by the same dewatering and drying procedures described above.

2.4. Microscopic imprinting

After being formed, patterning was done on the regenerated cellulose samples and evaluated using two simple approaches as proof-of-concept: 1) the sample was dried and imprinted using 304 stainless steel wire mesh (TIMESETL) at room temperature for 48 h with applied pressure; 2) a similar procedure as in 1 but using the 304 stainless steel wire mesh in the Rapid Köthen for 10 min at 93 °C and − 0,95 bar. The 304 stainless steel is a woven wire with 80 mesh and 0.17 mm holes.

2.5. Characterization

2.5.1. Solid content

The total solid content of the samples was measured by a KERN DBS moisture analyzer. In brief, the cellulose films and laminates were removed from the storage bag, and an appropriate squared fraction from each sample was cut and placed in the analyzer as fast as possible. Each sample was measured 4 times. The average values of moisture and solid contents are reported in Table S1 Supplementary data.

2.5.2. Atomic force microscopy

Surface morphology and roughness of the laminates were accessed by atomic force microscopy (AFM; Park Systems NX20, Korea). AFM was operated in a non-contact mode in air. A PPP-NCHR probe (Park Systems, Korea) with a nominal resonance frequency of 330 kHz and force constant of 42 N m^{-1} was used. AFM images of 50 × 50 μm^2

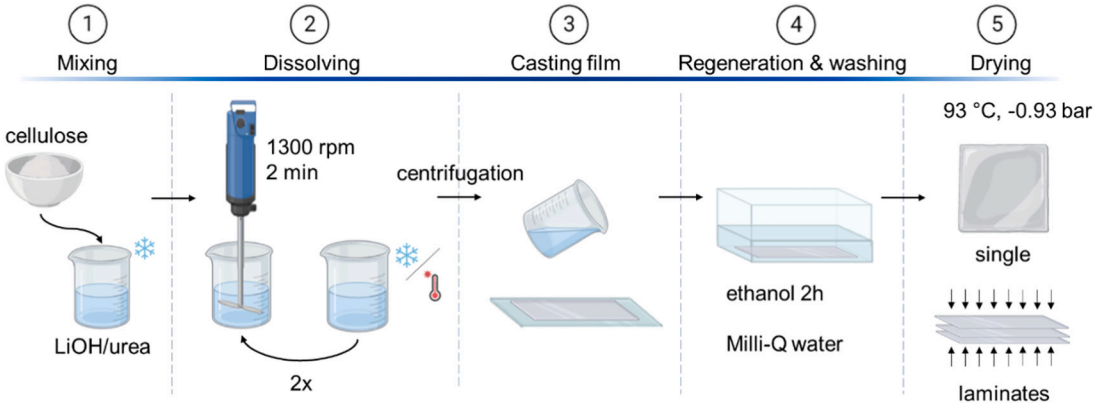

Fig. 1. Schematic illustration of the different steps highlighting the dissolution, regeneration of cellulose films and formation of the laminates. Note that for the films containing 10 wt% undissolved fibers, these were added to the cellulose dope prepared in step 2 before the regeneration (created with BioRender.com).

representative areas on the laminate samples were acquired with a scan rate of 0.3–0.6 Hz to gain >90 % matching of backward and forward scans. The surface roughness parameter (R_q) was determined using the Park Systems XEI 1.8.5 image analysis software.

2.5.3. Scanning electron microscopy

Field emission scanning electron microscopy (FE-SEM) imaging of the films and laminates was conducted using a TESCAN MAIA3 electron microscope in secondary electron (SE) mode with a 3 kV electron beam voltage. The working distance was 6 mm. The cross-sections were done using a Hitachi IM4000 Ion Milling System. The cellulose samples were coated with 2 nm Iridium using a Quorum Q150T ES before image acquisition. Surface and cross-section images were obtained for the laminates, while only surface images were obtained for the imprinted samples.

2.5.4. Fourier transform IR spectroscopy (FTIR)

The FTIR spectra of the laminates were obtained on a Thermo Scientific Nicolet 6700 spectrometer with the "Smart Orbit" diamond attenuated total reflectance (ATR). The samples were placed directly on the diamond ATR for analysis, and pressure was applied using a stainless steel pointed tip. All spectra were collected with OMNIC software in the region 400–4000 cm^{-1} with 4 cm^{-1} resolution and averaged over 32 scans.

2.5.5. X-ray diffraction analysis

X–ray diffraction (XRD) was carried out at room temperature using a Bruker D2 Phaser diffractometer with Cu Kα radiation (wavelength 1.54 Å) at 30 kV and 10 mA in θ–2θ geometry. The increment was fixed at 0.02°. The laminate specimens were placed on a silicon single crystal specially cut to provide a low background free from any interfering diffraction peaks. The XRD results on the replicate samples of each fabricated material were almost identical, with <10 % variation. The intensity values were only subtracted from the blank run intensity of the sample holder and presented.

2.5.6. Optical microscopy

Cellulose dopes were observed in an optical microscope (Leica M205 C) equipped with cross polarizers to infer the initial dissolution efficiency of the LiOH/urea system. Moreover, the optical microscopy was also used to investigate potential delamination when exposed to water. This was done by visualizing the cross section of the dry laminates and, after one week soaked in aqueous media. In brief, samples were marked to ensure the same region was analysed before and after swelling. 10 measurements were performed for both types of 3-layered laminates (CL3 and CFL3) before and after swelling. The magnification used was 16×.

2.5.7. Optical characterization: haze and transparency

The optical properties of the cellulose films were characterized using a standard setup for measuring haze (ASTM D1003–00). The setup consists of a halogen white light source (Ocean Optics), an integrating sphere, and a UV/visible spectrometer (Ocean Optics USB 2000+). Light from the white light source is guided to the integrating sphere using large core (600 μm) silica optical fibers. Light from the integrating sphere to the spectrometer is guided using a similar large core optical fiber. 5 mm squared samples of each cellulose laminate were cut and prepared to be placed at the entrance of the integrating sphere. The haze is calculated according to the relation below and requires four repeated measurements of each sample. The Haze-value is determined according to Eq. (1) as;

$$\text{Haze}\ (\%) = \left[\frac{T4}{T2} - \frac{T3}{T1}\right] \times 100 \quad (1)$$

T1 represents the incident light and is measured without a sample but by using a reflective (white) standard placed at the exit of the integrating sphere. T2 is the total light transmitted by the sample and is measured with the sample placed at the entrance and the reflective standard at the exit. T3 represents the scattered light by the instrument (integrating sphere) and is measured without both the sample and the reflective standard. Finally, T4 is the light scattered by both the instrument and the sample. T4 is measured with the sample placed at the entrance without the reflective standard at the exit.

2.5.8. Mechanical testing

Prior to the mechanical testing, all samples were conditioned at 23 °C and 50 % RH for 24 h according to ISO 187 (2020). Grammage (g m^{-2}) was measured according to ISO 536 (2020), and thickness (μm), density (kg m^{-3}), and bulk (g cm^{-3}) according to ISO 534 (2020). Tensile strength (kN m^{-1}), tensile index (kNm kg^{-1}), tensile stiffness (kN m^{-1}), tensile stiffness index (MNm kg^{-1}), tensile energy absorption (J m^{-2}), tensile energy absorption index (J kg^{-1}), strain at break (%) and E-modulus (Gpa) were performed following ISO 1924 (2020) using Tensile Tester, Code 066 (Lorensen & Wettre) and the sample size was 100 mm in length and 15 mm in width. Determination of the folding number (d) and folding strength (10-log) was done according to ISO 5626 (2020) using SE 006 Köhler Molin (Lorensen & Wettre) and the sample size was 200 mm in length and 15 mm in width.

2.5.9. Contact angle measurements

Water contact angle (WCA) measurements were conducted using the sessile drop method, employing the Dataphysics Instruments GmbH (model OCA20, Germany). Drops of 10 μL of distilled water were placed on the films. Six measurements were recorded for each sample.

2.5.10. Thermal gravimetric analysis

Thermal analysis was performed using a TGA Q500 TA thermal analyzer from TA instruments. The cellulose sample was heated under a nitrogen atmosphere (100 mL min^{-1}) from room temperature up to 600 °C at a rate of 10 °C min^{-1}. For a better normalization of the values, the char residue was estimated on a dry basis of material, that is, using the weight obtained after the thermogravimetric loss (at 150 °C) due to moisture and adsorbed water.

3. Results and discussion

The simple method introduced in this work results in surprisingly stable, flexible, and handable materials. As a proof of concept, laminates with 3 layers (ca. 200 μm thick) were formed and compared with single layer films (ca. 60 μm thick). Note that the simplicity of the process allows easy scaling, and therefore, thicker and stiffer laminates can be produced by increasing the number of regenerated cellulose films stacked. Initial trials have been successfully performed with up to 15 layers, but for proof-of-concept, only laminates with 3 layers will be considered in this work. Also, the initial thickness of one layer is possible to tune, and we managed to produce films with a thickness of <10 μm.

In Fig. 2, typical photographs of the formed laminates are shown. Their transparency, flexibility, and bendability are striking (Fig. 2a and b). Bendability data are presented in Table S2, Supplementary data. During the drying process, it is possible to tune the shape of the films at demand (for instance, a cupcake form is shown in Fig. 2c), which gives this material great potential to replace molded plastic packaging. Laminates can be easily shaped into different forms and a possible application is also displayed as environmentally friendly bio-clip used to hold, for instance, bags containing bread or cookies (Fig. 2d and e). It is worth mentioning that the bio-clip was punched out from the laminates without any delamination or artifacts.

The interactions between cellulose fibers are expected to greatly affect the adhesion, friction, swelling, and wetting properties, and hence the final properties of many products such as paper, textiles as well as the fiber containing laminates in this study. From a mechanism point of

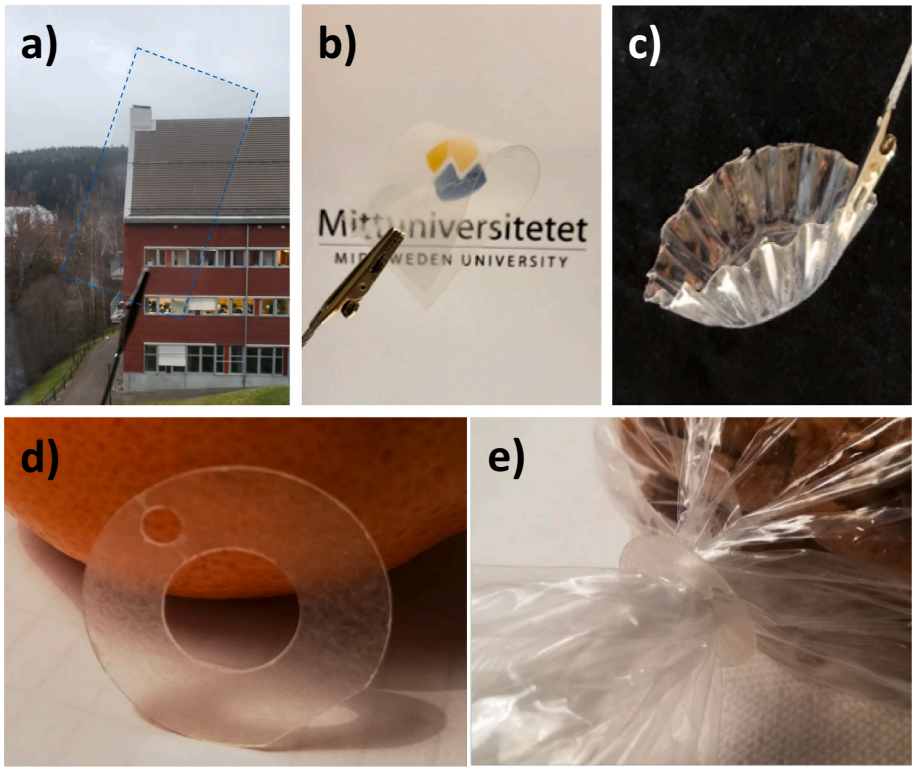

Fig. 2. All-cellulose laminates showing their a) high transparency, b) bendability, and c) flexibility. In photographs d) and e) a bread clip made with our all-cellulose fiber-containing laminate is shown.

view and as highlighted in the introduction, when the films are hydrated, cellulose fibers are in proximity but separated by water molecules; cellulose fibers interact mainly forming hydrogen bonds with water molecules at the cost of reducing the number of fiber–fiber hydrogen bonds (Wohlert et al., 2022). On the other hand, upon hot pressing and drying, cellulose fibers are forced to come into close contact and self-adhere displaying a large contact surface in the composite comprising the cellulose matrix-cellulose fiber structure (Li, Wang, et al., 2020; Roig-Sanchez et al., 2019; Ye et al., 2018).

It should be noted that since cellulose pulps have undergone extensive delignification and bleaching removing the lignin and most of the hemicelluloses (no beating of the pulp is applied in this work), a relatively low surface charge is expected. Thereby the repulsive component (due to the overlap of electric double layers of these fiber surfaces) will be relatively small in comparison to the van der Waals interactions. Thus, at intermediate surface separations sufficient to overcome the inherent roughness of natural fibers, the interaction energy will be net attractive. Therefore, once the hydration layer is disrupted or removed at high temperatures, close contact among cellulose molecules becomes possible, allowing for favorable intermolecular interactions; strong van der Waals interactions between cellulose fibers, along with mechanical interlocking, are thus expected to be pivotal in the formation mechanism of the laminates introduced in this work. These interactions significantly contribute to strengthening fiber-fiber joints in the laminates (Wohlert et al., 2022).

Apart from the physical interactions, covalent bond formation has also been suggested to occur upon hornification and laminate formation. However, given the mild experimental conditions used in our work (i.e., temperature of ca 93 °C), ester formation is very unlikely to occur. Such scenario is anticipated for harsher conditions (temperature $>$ 140 °C) and in the presence of acidic catalysts (Sellman et al., 2023). Moreover, the lack of significant changes in the FTIR intensities in the regions expected for hypothetical ester or hemiacetal crosslinks (around 1737 cm^{-1}), combined with the high transparency of the films (no colour change) and the observed delamination after prolonged exposure to water, further suggests that no chemical bonds are formed among the laminates. Overall, these results support that laminate formation mainly results from increased molecular contact/entanglements during drying which become reversible once exposed to water for a long time (Sellman et al., 2023).

The laminates were subjected to a series of analyses to elucidate their structure-property relationships. In Fig. 3a, the haze and total transmission of light are represented for CL1 and CL3 samples. All systems are highly transparent (above ca. 90 %) and display a very low haze, typically below 4 %. This can be ascribed to their compact structures (high density, see Table S2 in Supplementary data) and smooth surface, which facilitate light transmission without inducing strong light scattering. These remarkable optical properties are as high as observed in, for instance, cellulose nanofiber-based films (Fukuzumi et al., 2009; Kasuga et al., 2018; Nogi et al., 2009).

As mentioned, the optical properties correlate well with the smoothness and low surface roughness of the laminates, observed in the SEM micrograph (Fig. 3b). This is also corroborated by the AFM analysis (Fig. 3d), where the low R_q roughness parameter (i.e., R_q = 17 nm) agrees with R_q obtained in regenerated cellulose films in a series of different alcohols (Dahlström et al., 2024).

When comparing the obtained optical properties with other cellulose-based materials with potential application in food packaging, such as cellulose nanofibrils (CNF) and cellulose nanocrystals (CNC) based films and composites, it is possible to conclude that the films and laminates obtained in the present work are equal to or even more transparent. (Alves et al., 2022; Alves, Ramos, Ferraz, Ferreira, et al., 2023). The transmittance of CNF-based films was reported to be 89 %, while CNC-based films was 95 %, with corresponding haze of 77 % and 5 %, respectively (Li, Li, et al., 2020). The great optical properties of films and laminates obtained through dissolution and regeneration of cellulose could be somehow rationalized with the smaller dimensions of cellulose molecules or smaller aggregates obtained after cellulose

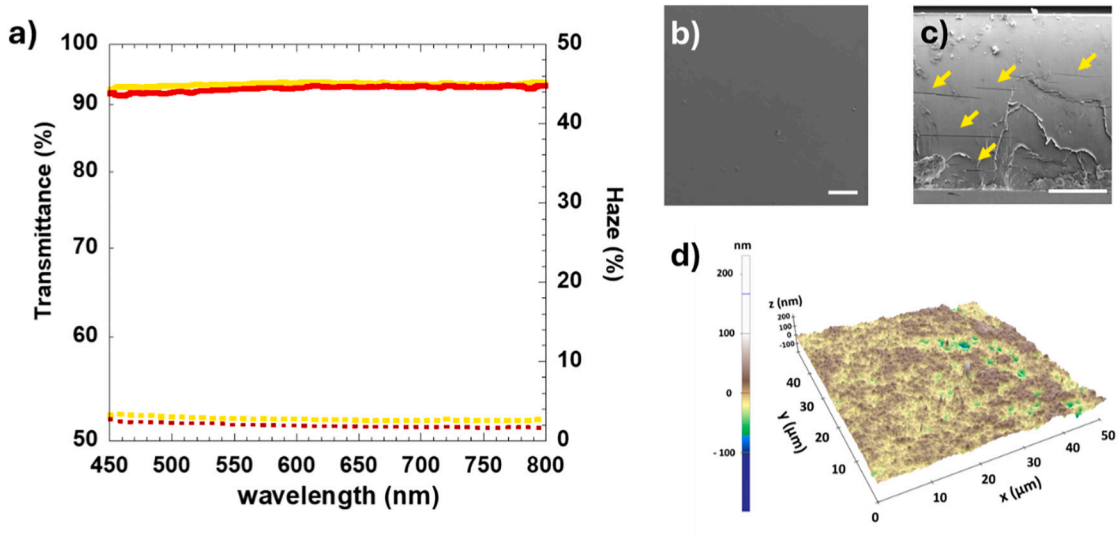

Fig. 3. a) Transmission (full curves) and Haze (dashed curves) of CL1 (yellow) and CL3 laminates (red). b) Scanning electron microscopy (SEM) top view image of the CL3 laminate (scale bar represents 200 μm) and c) cross-section of CL3 (scale bar represents 50 μm). d) Atomic force microscopy (AFM) 3D height images of the CL3 laminate.

dissolution, compared to the larger dimensions of CNC and CNF, which even for TEMPO-CNF with high levels of oxidation results in individual CNFs of several nanometers in diameter and hundreds of nanometers in length. This is more pronounced in the haze values that strongly depends on the film morphology. The packing of CNFs is poorer than the molecularly dissolved or small aggregates of cellulose, leading to films and laminates with improved optical properties, notwithstanding the laminates have larger thicknesses than the CNF films.

The SEM cross-section view shows "cracks" at different positions (highlighted by the yellow arrow heads in Fig. 3c). Since the observed cracks are not at the interface between the different layers but rather spread out in the bulk, it implies that the cellulose layers are strongly attached to each other after lamination. To be noted, these cracks might be artifacts arising from the high vacuum used in the cross-section polisher and SEM analysis. Overall, the CL3 samples present a remarkably homogenous cross-section.

As described in the experimental section, the formation of ACCs was evaluated by adding 10 wt% undissolved pulp fibers to the regenerated cellulose films before laminate formation. As mentioned, the amount of fibers used (i.e., 10 wt%) was purely selected for comparison purposes with the laminates without added fibers. In this work, there was no attempt to investigate the weight fraction role of added fibers in the properties of ACC laminates. As can be observed in Fig. 4, the roughness of the ACC laminate increases significantly with the addition of the fibers (R_q = 87 nm), which are clearly visible in the SEM micrograph.

The hydrophilicity of the systems was evaluated by water contact angle assays (Fig. 5). Overall, no significant changes are observed among single layer and 3 layer-samples, and all contact angles are well below 90° (hydrophilic films), which perfectly agrees with previous work (From et al., 2020). However, it is striking that systems with higher roughness (i.e., induced by adding undissolved fibers) present significantly lower contact angles, thus suggesting higher wettability of the ACCs. This can be rationalized by bearing in mind that the fibers added are rich in OH groups and by considering the relationship between roughness and wettability introduced by Wenzel (Wenzel, 1936). Essentially, such a relation states that the roughness is expected to accentuate the preexisting character of the material (i.e., hydrophilicity) with respect to the contact angle. It is important to note that since our films/laminates are hydrophilic, significant water uptake can occur, leading to substantial changes in surface roughness, surface energy, and wetting behavior. These changes may potentially invalidate the assumptions of the Wenzel theory. In such cases, a more comprehensive and reliable understanding of wetting behavior should consider models such as those proposed by Starov et al. (Starov & Velarde, 2019). In our experimental setup, the duration of contact angle measurements is relatively short, and the process of water absorption occurs considerably

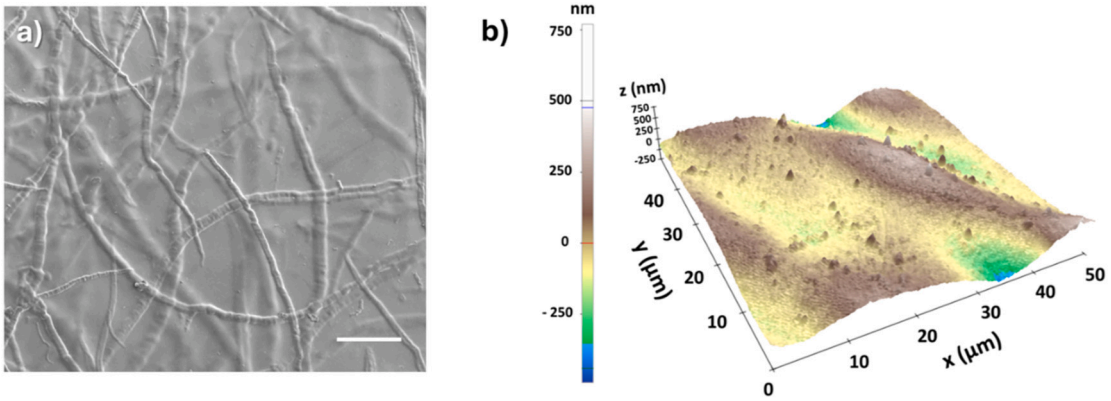

Fig. 4. a) Scanning electron microscopy (SEM) top view image of the CFL3 sample (scale bar represents 100 μm) and b) Atomic force microscopy (AFM) 3D height images of the CFL3 laminate.

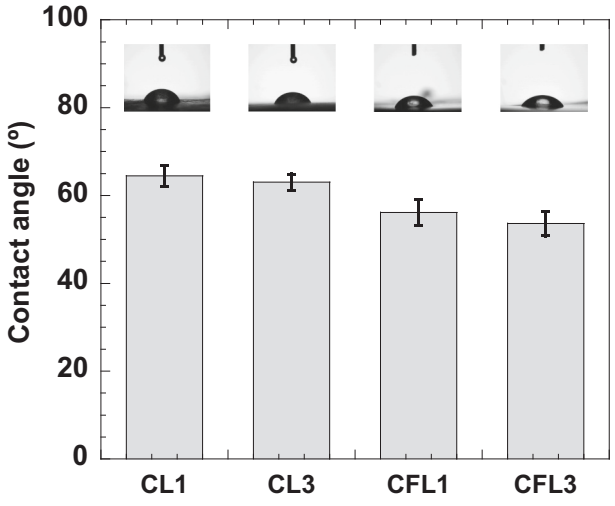

Fig. 5. Contact angle of cellulose films and laminates (samples CL1, CL3, CFL1 and CFL3). Inserted photos show the water drop at the surface of the different systems. The error bars represent the SD from six measurements.

slower compared to the timescale of contact angle measurements. Therefore, we consider the short-term contact angle measurements still valid for characterizing wetting behavior within a Wenzel framework.

As expected, the regenerated cellulose films are consistent with cellulose II allomorph (Fig. 6a). Such cellulose II allomorph crystallizes as monoclinic crystals with the unit cell containing chains arranged in an antiparallel fashion (Hori & Wada, 2006; Langan et al., 2001, 2005). The diffraction peaks are located at the diffraction angles (2θ) 12.6°, 20.6°, and 22.1°, corresponding to the crystallographic plane reflections (1−10), (110) and (020), respectively (From et al., 2020; Nam et al., 2016). Upon the laminate formation, the peak position does not shift. However, it is observed that increasing the thickness of the laminate (i.e., 3 layers vs. single films) enhances the intensity of the peaks. At a first glance, the cellulose I allomorph is not clearly detected in the diffractograms upon the addition of pristine cellulose fibers, even though the fibers can be clearly seen with the naked eye. Most likely, the minor contribution from these fibers with cellulose I crystalline organization is masked by the dominating cellulose II allomorph of regenerated films and leads to a noticeable increase in intensity in the assigned amorphous region (i.e., ~16° 2θ for cellulose II and ~ 18° 2θ for cellulose I allomorphs (Nam et al., 2016)), as the thickness and solid content of fabricated samples are almost identical (see Tables S1 and S3 in Supplementary data). In addition, adding fibers resulted in a slight increase in the intensity of overlapping crystalline peaks in the range of ~20–23° 2θ, which is expected due to a major intense peak of cellulose I at ~23° 2θ corresponding to (200) crystallographic plane (Nam et al., 2016). To further explore this, the diffractogram subtractions (e.g., CFL1 – CL1, CFL3 – CL3) were performed to probe the presence of cellulose I allomorph. Indeed, the resulting diffractogram clearly shows the crystalline peak of cellulose I at ~23° 2θ corresponding to (200) crystallographic plane (see Fig. S1). A similar conclusion can be reached from the FTIR analysis (Fig. 6b). The FTIR spectra of the laminates show characteristic bands of the cellulose structure; i.e., band at 1025 cm^{-1} (C—O stretching), 1139 cm^{-1} (C–O–C asymmetric stretching), 1184 cm^{-1} and 1210 cm^{-1} (–OH, –CH bending), 1316 cm^{-1} (CH_2 wagging), 1373 cm^{-1} (C—H bending), 2835–2980 cm^{-1} (CH and CH_2 stretching), 3447 cm^{-1} and 3488 cm^{-1} (–OH stretching intramolecular hydrogen bonds). Although the FTIR spectra can be sensitive to structural changes (e.g., different cellulose allomorph), again no evident crystalline cellulose I band arises. In fact, the observed bands at 3447 cm^{-1} and 3488 cm^{-1} can be assigned to the cellulose II allomorph (Carrillo et al., 2004). The penetration depth of the IR beam, low fraction of fibers and high intensity of characteristic cellulose II bands are thus expected to hide the cellulose I contributions.

To investigate the fiber-matrix interaction, the native fibers were also exposed to the alkali solvent, reproducing the conditions used for laminate formation (see experimental section for details). As shown in Fig. 7, the intensity of major crystalline peaks assigned to cellulose I decreases, while the cellulose II peaks, corresponding to the (1–10) and (110) crystallographic planes, emerge. This suggests the partial transition from cellulose I to the cellulose II allomorph. Therefore, it is reasonable to assume that when fibers are added to the cellulose dope before film regeneration, they may swell and rearrange to cellulose II during subsequent film casting and regeneration (Duchemin et al., 2016; Yang et al., 2010). Although no specific local probe or spatial resolved analysis was performed, it seems reasonable to assume that if any transformation is occurring on the fiber level, it is most likely happening first at the interface which is more accessible for the solvent. This process is anticipated to enhance not only the already high compatibility between fibers and cellulose matrix (as both are cellulose-based materials) but also facilitates possible co-crystallization between the fibers and the cellulose matrix upon regeneration (Dormanns et al., 2016; Kröling et al., 2018; Nishino & Arimoto, 2007). We believe this is supported by the remarkable mechanical features and absence of perceptible structural defects at the fiber/matrix interface. SEM analysis does suggest that fibers are perfectly embedded in the matrix.

The thermal properties of the single layer and cellulose laminates were accessed by TGA analysis (Fig. 8). No significant differences are noticed since all systems are essentially composed of cellulose.

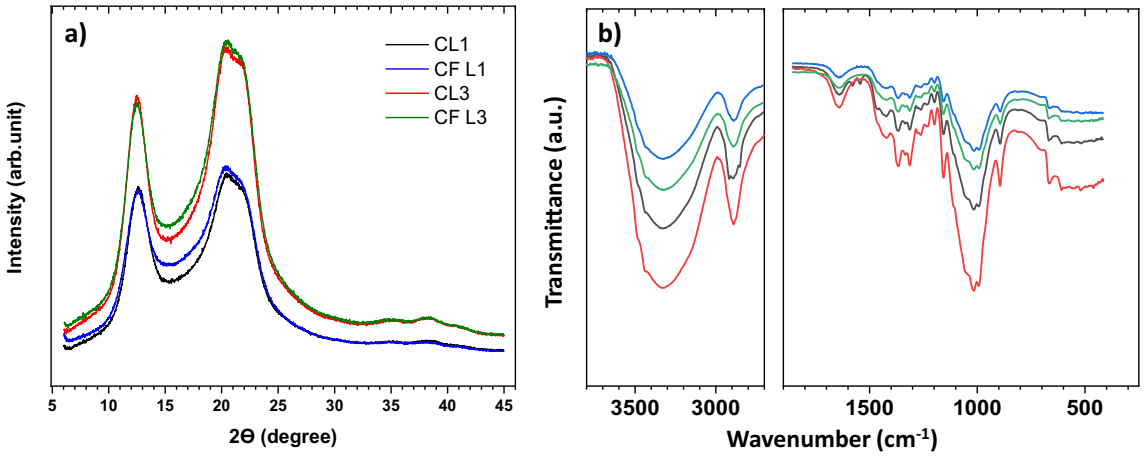

Fig. 6. a) X-ray diffraction (XRD) patterns, and b) FTIR of different cellulose systems: CL1 (black curve), CL3 (red curve), CFL1 (blue curve), and CFL3 (green curve).

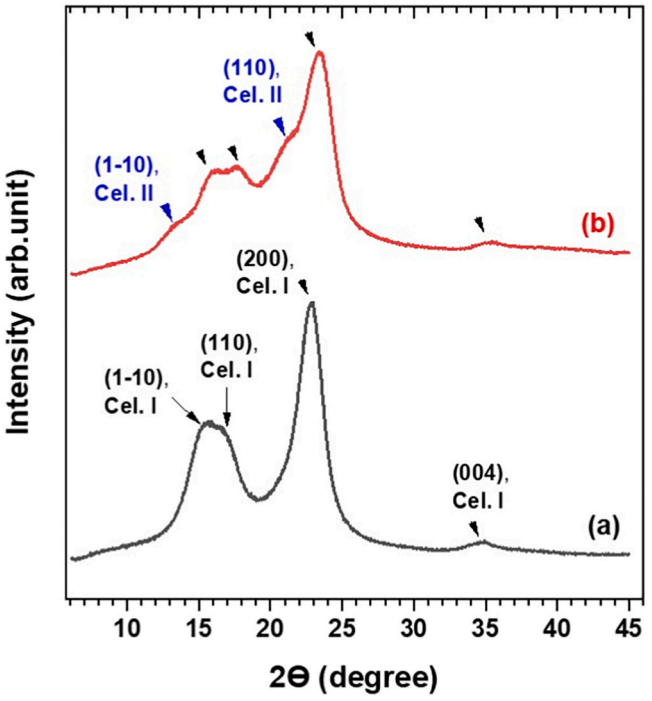

Fig. 7. XRD patterns of (a) reference kraft pulp, (b) kraft pulp treated with 4.6 wt% LiOH and 15 wt% urea for 2 h. The samples thickness were identical. The black arrow head denote the principal crystalline peaks for the allomorph cellulose I (Cel.I), while the blue arrow heads refer to the crystalline peaks for the allomorph cellulose II (Cel. II).

Nevertheless, some facts are worth discussing. The first observation is that single layer films have an initial more significant drop in weight (i.e., up to 200 °C) than the 3-layered laminates. This might be related to the larger thickness of 3-layer laminates, which delays the evaporation of volatile compounds and residual moisture. On the other hand, the addition of pristine pulp fibers to the laminates shifts the transition temperature ca. 5 °C (see insert in Fig. 8b). This minor shift to higher temperatures is most likely due to the enhanced thermal stability of cellulose I in comparison to cellulose II (Poletto et al., 2011).

The mechanical features of the cellulose laminates were determined, and several relevant parameters were compiled in Table S2 (Supplementary data). The typical stress-strain curves of the single and 3-layer laminates (without fibers) are shown in Fig. S2. In Fig. 9, an Ashby-like plot is presented relating the Young's modulus and density of different classes of materials (Ashby, 2011). The laminates developed in this work present a density comparable to elastomers and polymers but with a Young's modulus remarkably higher than common polymers (see Table S2 for details). For instance, the Young's modulus of polystyrene (ca. 3 GPa), polypropylene (ca. 1.5 GPa) and polyethylene (<1 GPa) are considerably lower than the Young's modulus of single layer films (ca. 9 GPa). The presence of 10 wt% fibers decreases the Young's modulus on single layer films down to ca. 7 GPa. A similar value is observed for the 3-layer laminates with undissolved fibers. The modulus obtained for the materials in the present work are also superior when compared to the values reported for CNF films (Alves et al., 2022; Alves, Ramos, Ferraz, Ferreira, et al., 2023; Alves, Ramos, Ferraz, Sanguino, et al., 2023). The way the particles/molecules can join and interact deeply impacts the properties of the materials, namely in the mechanical properties. This could explain why the films and laminates prepared through cellulose dissolution and regeneration present a higher Young's modulus than CNF-based films and why the Young's modulus of the films and laminates containing undissolved fibers showed a reduction in this property. From Table S2, one can also observe that the tensile stiffness increases considerably when 3-layer laminates are formed.

Adding to the very favorable mechanical properties, the laminates can be patterned. A simple proof-of-concept is shown in Fig. 10. As described in the experimental section, the laminate patterning was

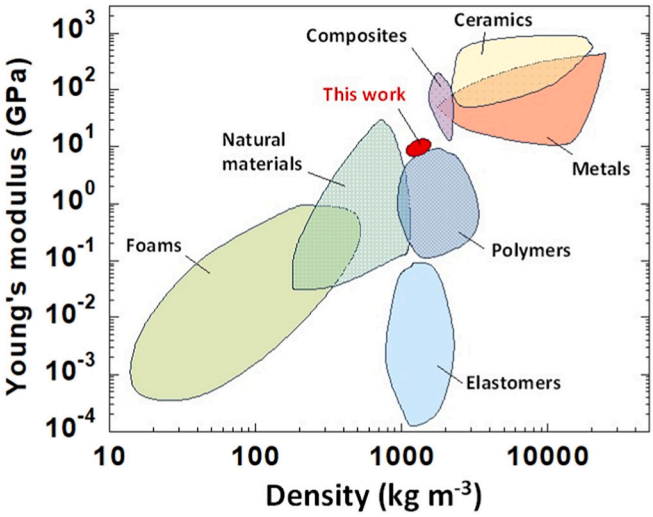

Fig. 9. Ashby plot of Young's modulus vs. density for different classes of materials. The systems developed in this work are highlighted in the red area. (Adapted and modified with permission from (Ashby, 2011)).

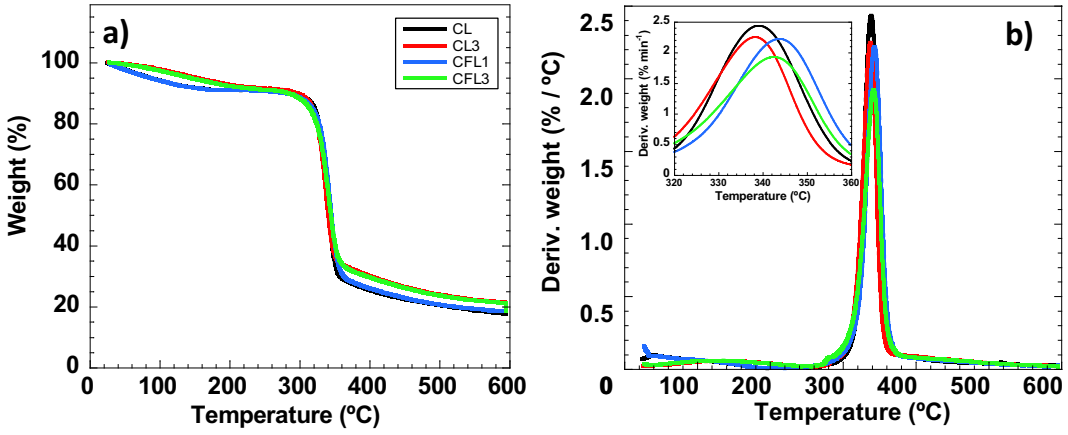

Fig. 8. a) Thermograms and the corresponding b) differential thermograms of cellulose laminates: CL1 (black curve), CL3 (red curve), CFL1 (blue curve) and CFL3 (green curve). The insert in the derivative plot highlights the peak shift and consequent difference in the main transition temperature.

performed with a stainless-steel wire mesh, and two approaches were tested: "fast procedure" (imprinting executed in a Rapid Köthen, for 10 min at 93 °C and − 0.95 bar) and "slow procedure" (imprinting performed at room temperature, for 48 h under pressure). As can be observed in Fig. 10, the imprinting works remarkably well, particularly for the "slow procedure", with striking well-defined "valleys" and "peaks". Images with higher magnification and different mesh sizes are reported in Fig. S3 in the Supplementary data. Overall, data suggests that these simple soft lithography-like procedures can efficiently imprint precise topographic patterns on the cellulose laminates. It is important to choose a suitable template for imprinting depending on the target application.

A direct consequence of such microscopic imprinting is the change in surface wettability. While the original 3-layer laminate presented a contact angle of ca. 63°, the laminates with topographical patterning showed a considerable decrease in their contact angle (i.e., laminate side with "valleys" present a contact angle of ca. 46° while the side with "peaks" display a contact angle of ca. 32°). As patterning induces surface roughness, the laminate hydrophilicity tends to be accentuated (similar to the roughness induced by adding undissolved cellulose fibers). Moreover, the capillary forces arising from the pattern may further favor water penetration, which, coupled with surface hydrophilicity, results in a Wenzel regime where water is absorbed, decreasing the contact angle (Krainer & Hirn, 2021). As previously mentioned, other models might be more suitable for rationalizing the wetting behavior. The heterogeneous nature of solid surfaces, manifested in either geometric (roughness) or chemical (variation in surface energy across different regions of the surface) aspects, is important, but other effect, such as surface (disjoining pressure) and capillary forces, should be considered when analyzing the wetting phenomenon (Starov & Velarde, 2019). Recent studies have shown that it is possible to tune the contact angle by changing the micropatterning; as shapes become larger and better defined, the capillary action is enhanced, and the contract angle decreases. Most likely, this is contributing to a lower contact angle of the "peaks" surface in comparison to the "valleys" (Banvillet et al., 2023). With an optimized imprinting template, it should be possible to mimic the surface of e.g. the lotus leaf providing a hydrophobic surface or even superhydrophobic surface with additional chemical modifiations.

The swellability and delamination of the cellulose laminates (with and without added fibers) were evaluated by optical microscopy (cross-section thickness) over 1 week in milliQ water (Fig. 11). The laminates without fibers present a thickness increase of ca. 66 %, while the laminates containing fibers increased their thickness by 94 %. As shown in Fig. 11b, delamination occurs preferentially in between the top two of the layers; a significant part of the swelling is due to the increased water content between the layers, but it seems that some swelling also occurs within the layers. It should be noted that even though there is an obvious swelling of the laminate after one week, the samples are still stable and do not delaminate without applied force. The laminates containing fibers exhibit a less uniform thickness, as anticipated. Additionally, swelling is much more pronounced in these samples as more micro structural defects are expected, which are prone to enhance water uptake. A similar qualitative behavior was observed for the single layer films. The dry and wet thickness of all systems is compiled in Table S3.

The water uptake (weight gain over time) was evaluated in both pure and high saline water (mimicking salt concentration in the Atlantic Sea, ca. 0.6 M) (Fig. 12). Although it was not the goal of this work to delve into the swelling mechanisms, the data could be fitted to a first order

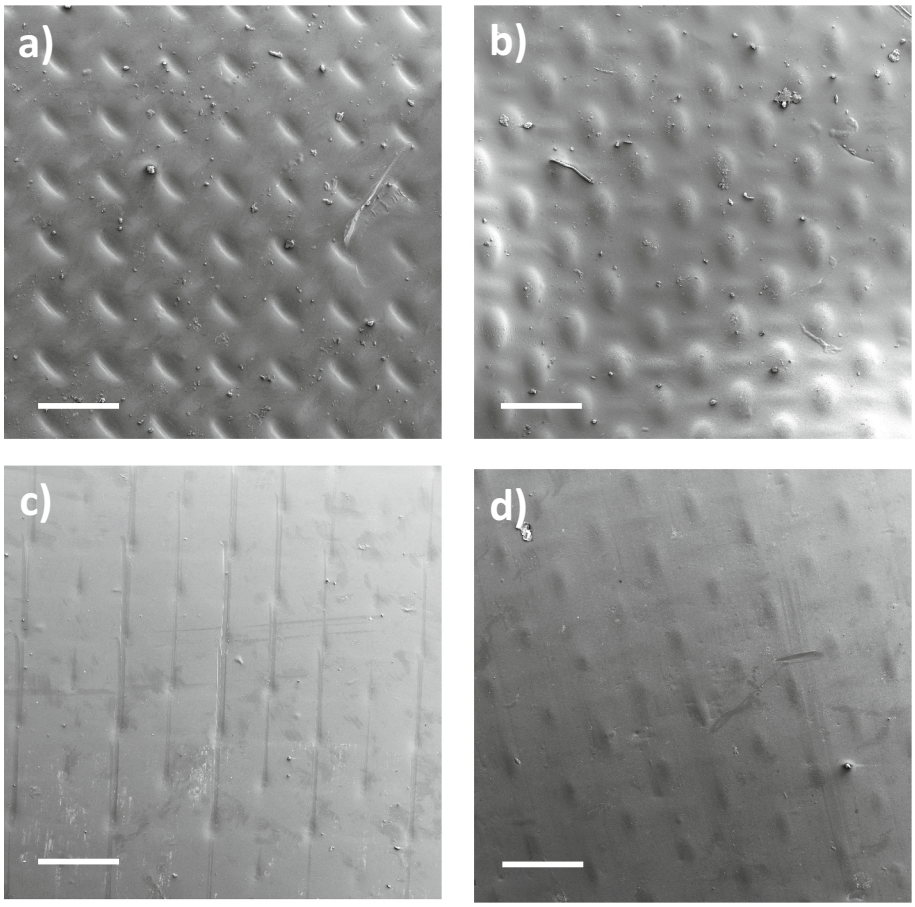

Fig. 10. SEM micrographs of CL1 patterned using a stainless-steel wire mesh. a) and b) refer to the "slow procedure" (imprinting executed at room temperature, for 48 h under pressure) while c) and d) refer to the "fast procedure" (imprinting executed in a Rapid Köthen, for 10 min at 93 °C and − 0.95 bar). Both "valleys" (a and c) and "peaks" (b and d) are observed. The scale bars represent 500 μm.

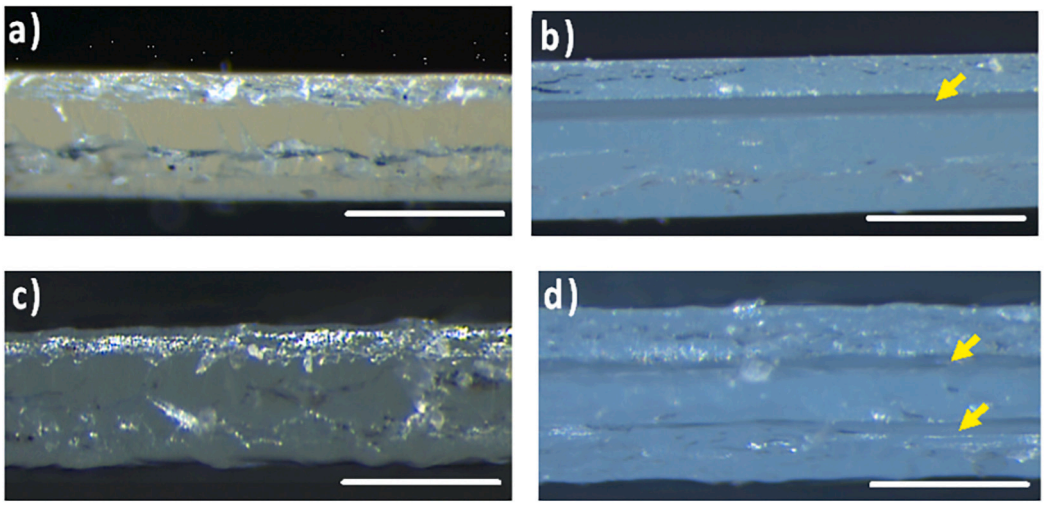

Fig. 11. Optical light microscopy images of cross section on dry laminates (a and c) and wet laminates (b and d). The laminates without fibers (CL samples) are in panels a and b, while those containing 10 wt% undissolved fibers (CLF samples) are in panels c and d. The yellow arrow heads show the preferential water swelling and delamination occurring in-between cellulose layers. The scale bars represent 250 μm.

kinetic model, which is commonly expressed in Eq. (2);

$$M(t) = M_0.\left(1 - e^{kt}\right) \quad (2)$$

where M(t) is the mass of the laminate at time t, M_0 is the initial mass of the laminate, and k is the first-order rate constant. The swelling of cellulose fibers has generally been described as the swelling of a polyelectrolyte gel, where the weak acidic groups within the fiber wall may create an osmotic pressure, giving rise to a fiber wall expansion. This swelling is affected by both changes in electrolyte concentration and pH changes (Ahola et al., 2008; Fält et al., 2003). The cellulose structure contains many hydroxyl groups, making it prone to forming hydrogen bonds with water molecules. From Fig. 12, it is clear that the weight gain is enhanced for the laminates in pure water, while a low water uptake is observed in the saline water. This difference can be rationalized by considering that the cellulose films interact strongly with pure water through hydrogen bonding, leading to increased water absorption and swelling. On ther other hand, in saline water, the presence of dissolved salts increases the osmotic pressure outside the cellulose laminate, which can limit the influx of solvent since water molecules need to overcome the osmotic pressure created by the dissolved salts.

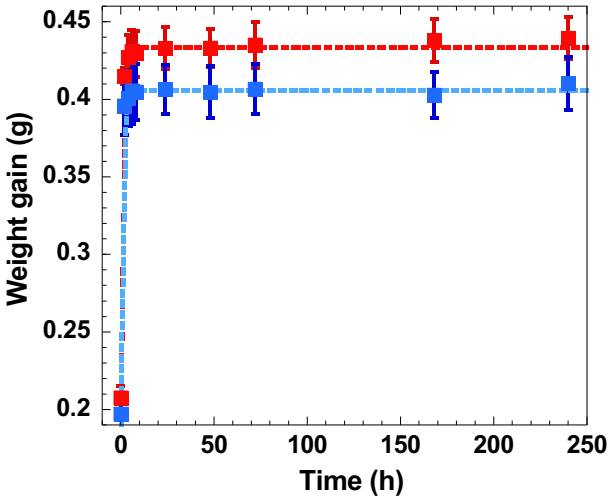

Fig. 12. Swelling kinetics of CL3 laminates in pure water (red squares) and in simulated sea water (blue squares). The dashed lines are the best fitting to Eq. (2). Error bars represent the standard deviation of 3 samples.

Additionally, the high concentration of ions in saline water may alter the interaction between water molecules and the cellulose surface, reducing the swelling effect compared to pure water. The ions in the saline water may also screen some existing charges in the laminate films, which will further contribute to a lower laminate swelling. According to Grignon and Scallan (Grignon & Scallan, 1980), there is a large decrease in the swelling forces when the salt concentration is high (above ca. 10^{-3} M for NaCl). Hence, this indicates that when the swelling pressure is decreased at salt concentrations larger than 10^{-3} M, there will be only minor changes in the adsorbed amount of water, and the rate of these changes will also be lower.

4. Conclusion

The all-cellulose laminates concept introduced in this work perfectly aligns with the global shift towards eco-friendly, renewable, and biodegradable materials that can replace traditional synthetic composites, contributing to a more sustainable future. A simple procedure is described relying on the stacking of regenerated cellulose II films without the need for solvents (for impregnation and/or partial dissolution), chemical modifications, or resins. As a proof-of concept, thin and flexible (with just one layer) or thick and rigid (with three layers) systems were formed. The procedure allows the possibility of easily tuning the number of films to be stacked. From a mechanistic viewpoint, the laminate formation and cohesion are argued to take advantage of the self-aggregation forces mainly arising from non-polar interactions and hydrogen bonding between regenerated cellulose films upon dehydration (hot pressing). The ACC laminates formed are highly transparent, have low haze, and present favorable mechanical properties (comparable or superior to traditional plastics). The laminates are relatively stable, and delamination only occurs after prolonged exposure to aqueous media. The laminates are malleable and can be easily imprinted (microscopic patterning). Such micropatterning affects the surface wettability of the laminates (becoming more hydrophilic). The easiness of micropatterning may play a critical role in many scientific and technological fields since it enables precise control and manipulation at small scales, representing an essential feature for various applications ranging from electronics to biotechnology and materials science. Undissolved fibers can be added to the laminates without compromising their characteristics. Overall, these innovative all-cellulose laminates present a robust, eco-friendly alternative to traditional synthetic materials, thus bridging the gap between environmental responsibility and high-performance functionality.

CRediT authorship contribution statement

Christina Dahlström: Writing – review & editing, Writing – original draft, Visualization, Validation, Investigation, Conceptualization. **Ran Duan:** Writing – review & editing, Investigation. **Alireza Eivazi:** Writing – review & editing, Investigation. **Solange Magalhães:** Investigation. **Luís Alves:** Writing – review & editing. **Ida Svanedal:** Writing – review & editing, Investigation. **Håkan Edlund:** Writing – review & editing. **Bruno Medronho:** Writing – review & editing, Writing – original draft. **Magnus Norgren:** Writing – review & editing.

Declaration of competing interest

The authors declare that they have no known competing financial interests or personal relationships that could have appeared to influence the work reported in this paper.

Data availability

Data will be made available on request.

Acknowledgements

The authors are grateful for the financial support from the KK Foundation and the European Regional Development Fund (grant number 20361245). This research has been supported by Treesearch. BM acknowledges the Portuguese Foundation for Science and Technology (FCT) through the projects UIDB/05183/2020 and the researcher grant CEECIND/01014/2018/CP1540/CT0002 (DOI: 10.54499/CEECIND/01014/2018/CP1540/CT0002). S.M. acknowledges the Portuguese Foundation for Science and Technology for the PhD grant 2020.07638.BD. L.A. acknowledges FCT for the research grant 2021.00399. CEECIND (DOI: 10.54499/2021.00399.CEECIND/CP1656/CT0025). The Strategic Research Center Project UIDB00102/2020, funded by FCT, is also acknowledged.

Appendix A. Supplementary data

Supplementary data to this article can be found online at https://doi.org/10.1016/j.carbpol.2024.122523.

References

Ahola, S., Salmi, J., Johansson, L.-S., Laine, J., & Österberg, M. (2008). Model films from native cellulose nanofibrils. Preparation, swelling, and surface interactions. *Biomacromolecules, 9*(4), 1273–1282. https://doi.org/10.1021/bm701317k

Alves, L., Ramos, A., Ferraz, E., Ferreira, P. J. T., Rasteiro, M. G., & Gamelas, J. A. F. (2023). Design of cellulose nanofibre-based composites with high barrier properties. *Cellulose, 30*(16), 10157–10174. https://doi.org/10.1007/s10570-023-05495-z

Alves, L., Ramos, A., Ferraz, E., Sanguino, P., Santarén, J., Rasteiro, M. G., & Gamelas, J. A. F. (2023). Effect of the dispersion state of minerals on the properties of cellulose nanofiber-based composite films. *Applied Clay Science, 233*, Article 106823. https://doi.org/10.1016/j.clay.2023.106823

Alves, L., Ramos, A., Rasteiro, M. G., Vitorino, C., Ferraz, E., Ferreira, P. J. T., … Gamelas, J. A. F. (2022). Composite films of nanofibrillated cellulose with Sepiolite: Effect of preparation strategy. *Coatings, 12*(3), 303. https://doi.org/10.3390/coatings12030303

Ashby, M. F. (2011). *Materials Selection in Mechanical Design* (4th ed.). Elsevier. https://doi.org/10.1016/B978-1-85617-663-7.00004-7 (Chapter 4).

Baghaei, B., & Skrifvars, M. (2020). All-cellulose composites: A review of recent studies on structure, properties and applications. *Molecules, 25*(12), 2836. https://doi.org/10.3390/molecules25122836

Banvillet, G., Pritchard, S., Kaschuk, J. J., Shi, X., Imani, M., Lu, Y., … Rojas, O. J. (2023). Monolithic nanocellulose films patterned with flower-shaped and other microstructures: A facile route to modulate topographical, wetting and optical properties. *Materials Today Nano, 24*, Article 100424. https://doi.org/10.1016/j.mtnano.2023.100424

Baranov, A., Sommerhoff, F., Duchemin, B., Curnow, O., & Staiger, M. P. (2021). Toward a facile fabrication route for all-cellulose composite laminates via partial dissolution in aqueous tetrabutylphosphonium hydroxide solution. *Composites Part A: Applied Science and Manufacturing, 140*, Article 106148. https://doi.org/10.1016/j.compositesa.2020.106148

Cai, J., & Zhang, L. (2005). Rapid dissolution of cellulose in LiOH/urea and NaOH/urea aqueous solutions. *Macromolecular Bioscience, 5*(6), 539–548. https://doi.org/10.1002/mabi.200400222

Carrillo, F., Colom, X., Suñol, J., & Saurina, J. (2004). Structural FTIR analysis and thermal characterisation of lyocell and viscose-type fibres. *European Polymer Journal, 40*(9), 2229–2234. https://doi.org/10.1016/j.eurpolymj.2004.05.003

Dahlström, C., Eivazi, A., Nejström, M., Zhang, R., Pettersson, T., Iftikhar, H., … Norgren, M. (2024). Regenerated cellulose properties tailored for optimized triboelectric output and the effect of counter-tribolayers. *Cellulose, 31*, 2047–2061. https://doi.org/10.1007/s10570-024-05745-8

Dormanns, J. W., Schuermann, J., Müssig, J., Duchemin, B. J. C., & Staiger, M. P. (2016). Solvent infusion processing of all-cellulose composite laminates using an aqueous NaOH/urea solvent system. *Composites Part A: Applied Science and Manufacturing, 82*, 130–140. https://doi.org/10.1016/j.compositesa.2015.12.002

Duchemin, B., Le Corre, D., Leray, N., Dufresne, A., & Staiger, M. P. (2016). All-cellulose composites based on microfibrillated cellulose and filter paper via a NaOH-urea solvent system. *Cellulose, 23*(1), 593–609. https://doi.org/10.1007/s10570-015-0835-4

Fält, S., Wågberg, L., & Vesterlind, E.-L. (2003). Swelling of model films of cellulose having different charge densities and comparison to the swelling behavior of corresponding fibers. *Langmuir, 19*(19), 7895–7903. https://doi.org/10.1021/la026984i

From, M., Larsson, P. T., Andreasson, B., Medronho, B., Svanedal, I., Edlund, H., & Norgren, M. (2020). Tuning the properties of regenerated cellulose: Effects of polarity and water solubility of the coagulation medium. *Carbohydrate Polymers, 236*, Article 116068. https://doi.org/10.1016/j.carbpol.2020.116068

Fukuzumi, H., Saito, T., Iwata, T., Kumamoto, Y., & Isogai, A. (2009). Transparent and high gas barrier films of cellulose nanofibers prepared by TEMPO-mediated oxidation. *Biomacromolecules, 10*(1), 162–165. https://doi.org/10.1021/bm801065u

Gericke, M., Amaral, A. J. R., Budtova, T., De Wever, P., Groth, T., Heinze, T., … Fardim, P. (2024). The European Polysaccharide Network of Excellence (EPNOE) research roadmap 2040: Advanced strategies for exploiting the vast potential of polysaccharides as renewable bioresources. *Carbohydrate Polymers, 326*, Article 121633. https://doi.org/10.1016/j.carbpol.2023.121633

Grignon, J., & Scallan, A. M. (1980). Effect of pH and neutral salts upon the swelling of cellulose gels. *Journal of Applied Polymer Science, 25*(12), 2829–2843. https://doi.org/10.1002/app.1980.070251215

Hori, R., & Wada, M. (2006). The thermal expansion of cellulose II and IIII crystals. *Cellulose, 13*(3), 281–290. https://doi.org/10.1007/s10570-005-9038-8

Huber, T., Müssig, J., Curnow, O., Pang, S., Bickerton, S., & Staiger, M. P. (2012). A critical review of all-cellulose composites. *Journal of Materials Science, 47*(3), 1171–1186. https://doi.org/10.1007/s10853-011-5774-3

Huber, T., Pang, S., & Staiger, M. P. (2012). All-cellulose composite laminates. *Composites Part A: Applied Science and Manufacturing, 43*(10), 1738–1745. https://doi.org/10.1016/j.compositesa.2012.04.017

Jayme, G., & Hunger, G. (1956). Verhornungserscheinungen an Cellulosefaserstrukturen in elektronenoptischer Sicht. *Monatshefte für Chemie, 87*(1), 8–23. https://doi.org/10.1007/BF00903586

Kalka, S., Huber, T., Steinberg, J., Baronian, K., Müssig, J., & Staiger, M. P. (2014). Biodegradability of all-cellulose composite laminates. *Composites Part A: Applied Science and Manufacturing, 59*, 37–44. https://doi.org/10.1016/j.compositesa.2013.12.012

Kasuga, T., Isobe, N., Yagyu, H., Koga, H., & Nogi, M. (2018). Clearly transparent nanopaper from highly concentrated cellulose nanofiber dispersion using dilution and sonication. *Nanomaterials, 8*(2), 104. https://doi.org/10.3390/nano8020104

Klemm, D., Heublein, B., Fink, H.-P., & Bohn, A. (2005). Cellulose: Fascinating biopolymer and sustainable raw material. *Angewandte Chemie International Edition, 44*(22), 3358–3393. https://doi.org/10.1002/anie.200460587

Krainer, S., & Hirn, U. (2021). Contact angle measurement on porous substrates: Effect of liquid absorption and drop size. *Colloids and Surfaces A: Physicochemical and Engineering Aspects, 619*, Article 126503. https://doi.org/10.1016/j.colsurfa.2021.126503

Kröling, H., Duchemin, B., Dormanns, J., Schabel, S., & Staiger, M. P. (2018). Mechanical anisotropy of paper-based all-cellulose composites. *Composites Part A: Applied Science and Manufacturing, 113*, 150–157. https://doi.org/10.1016/j.compositesa.2018.07.005

Labidi, K., Korhonen, O., Zrida, M., Hamzaoui, A. H., & Budtova, T. (2019). All-cellulose composites from alfa and wood fibers. *Industrial Crops and Products, 127*, 135–141. https://doi.org/10.1016/j.indcrop.2018.10.055

Langan, P., Nishiyama, Y., & Chanzy, H. (2001). X-ray structure of mercerized cellulose II at 1 Å resolution. *Biomacromolecules, 2*(2), 410–416. https://doi.org/10.1021/bm005612q

Langan, P., Sukumar, N., Nishiyama, Y., & Chanzy, H. (2005). Synchrotron X-ray structures of cellulose Iβ and regenerated cellulose II at ambient temperature and 100 K. *Cellulose, 12*(6), 551–562. https://doi.org/10.1007/s10570-005-9006-3

Li, H., Roth, S. V., Freychet, G., Zhernenkov, M., Asta, N., Wågberg, L., & Pettersson, T. (2021). Structure development of the interphase between drying cellulose materials revealed by in situ grazing-incidence small-angle X-ray scattering. *Biomacromolecules, 22*(10), 4274–4293. https://doi.org/10.1021/acs.biomac.1c00845

Li, X., Wang, M., Zhang, X., Chang, H., Wang, Y., & Zhang, Z. (2020). Optical haze regulation of cellulose nanopaper via morphological tailoring and nano-hybridization of cellulose nanoparticles. *Cellulose, 27*, 1315–1326. https://doi.org/10.1007/s10570-019-02876-1

Li, Z., Li, X., Ren, J., Wu, B., Luo, Q., Liu, X., & Pei, C. (2020). Robust all-cellulose nanofiber composite from stack-up bacterial cellulose hydrogels via self-aggregation

forces. *Journal of Agricultural and Food Chemistry, 68*(9), 2696–2701. https://doi.org/10.1021/acs.jafc.9b07671
Lindman, B., Medronho, B., Alves, L., Costa, C., Edlund, H., & Norgren, M. (2017). The relevance of structural features of cellulose and its interactions to dissolution, regeneration, gelation and plasticization phenomena. *Physical Chemistry Chemical Physics, 19*(35), 23704–23718. https://doi.org/10.1039/C7CP02409F
Lindman, B., Medronho, B., Alves, L., Norgren, M., & Nordenskiöld, L. (2021). Hydrophobic interactions control the self-assembly of DNA and cellulose. *Quarterly Reviews of Biophysics, 54*, Article e3. https://doi.org/10.1017/S0033583521000019
Lindman, B., Medronho, B., & Theliander, H. (2015). Editorial: Cellulose dissolution and regeneration: Systems and interactions. *Nordic Pulp & Paper Research Journal, 30*(1), 2–3. https://doi.org/10.3183/npprj-2015-30-01-p002-003
Medronho, B., & Lindman, B. (2014). Competing forces during cellulose dissolution: From solvents to mechanisms. *Current Opinion in Colloid & Interface Science, 19*(1), 32–40. https://doi.org/10.1016/j.cocis.2013.12.001
Medronho, B., & Lindman, B. (2015). Brief overview on cellulose dissolution/regeneration interactions and mechanisms. *Advances in Colloid and Interface Science, 222*, 502–508. https://doi.org/10.1016/j.cis.2014.05.004
Mo, W., Chen, K., Yang, X., Kong, F., Liu, J., & Li, B. (2022). Elucidating the hornification mechanism of cellulosic fibers during the process of thermal drying. *Carbohydrate Polymers, 289*, Article 119434. https://doi.org/10.1016/j.carbpol.2022.119434
Nam, S., French, A. D., Condon, B. D., & Concha, M. (2016). Segal crystallinity index revisited by the simulation of X-ray diffraction patterns of cotton cellulose Iβ and cellulose II. *Carbohydrate Polymers, 135*, 1–9. https://doi.org/10.1016/j.carbpol.2015.08.035
Nilsson, H., Galland, S., Larsson, P. T., Gamstedt, E. K., Nishino, T., Berglund, L. A., & Iversen, T. (2010). A non-solvent approach for high-stiffness all-cellulose biocomposites based on pure wood cellulose. *Composites Science and Technology, 70*(12), 1704–1712. https://doi.org/10.1016/j.compscitech.2010.06.016
Nishino, T., & Arimoto, N. (2007). All-cellulose composite prepared by selective dissolving of fiber surface. *Biomacromolecules, 8*(9), 2712–2716. https://doi.org/10.1021/bm0703416
Nishino, T., Matsuda, I., & Hirao, K. (2004). All-cellulose composite. *Macromolecules, 37*(20), 7683–7687. https://doi.org/10.1021/ma049300h
Nogi, M., Iwamoto, S., Nakagaito, A. N., & Yano, H. (2009). Optically transparent nanofiber paper. *Advanced Materials, 21*(16), 1595–1598. https://doi.org/10.1002/adma.200803174
Notley, S. M., Pettersson, B., & Wågberg, L. (2004). Direct measurement of attractive van der Waals' forces between regenerated cellulose surfaces in an aqueous environment. *Journal of the American Chemical Society, 126*(43), 13930–13931. https://doi.org/10.1021/ja045992d
Poletto, M., Pistor, V., Zeni, M., & Zattera, A. J. (2011). Crystalline properties and decomposition kinetics of cellulose fibers in wood pulp obtained by two pulping processes. *Polymer Degradation and Stability, 96*(4), 679–685. https://doi.org/10.1016/j.polymdegradstab. 2010.12.007
Qi, H., Cai, J., Zhang, L., & Kuga, S. (2009). Properties of films composed of cellulose nanowhiskers and a cellulose matrix regenerated from alkali/urea solution. *Biomacromolecules, 10*(6), 1597–1602. https://doi.org/10.1021/bm9001975
Roig-Sanchez, S., Jungstedt, E., Anton-Sales, I., Malaspina, D. C., Faraudo, J., Berglund, L. A., … Roig, A. (2019). Nanocellulose films with multiple functional nanoparticles in confined spatial distribution. *Nanoscale Horizons, 4*(3), 634–641. https://doi.org/10.1039/C8NH00310F
Sellman, F. A., Benselfelt, T., Larsson, P. T., & Wågberg, L. (2023). Hornification of cellulose-rich materials – A kinetically trapped state. *Carbohydrate Polymers, 318*, Article 121132. https://doi.org/10.1016/j.carbpol.2023.121132
Sjöstrand, B., Karlsson, C.-A., Barbier, C., & Henriksson, G. (2023). Hornification in commercial chemical pulps: Dependence on water removal and hornification mechanisms. *BioResources, 18*(2), 3856–3869. https://doi.org/10.15376/biores.18.2.3856-3869
Song, J., Chen, C., Zhu, S., Zhu, M., Dai, J., Ray, U., … Hu, L. (2018). Processing bulk natural wood into a high-performance structural material. *Nature, 554*(7691), 224–228. https://doi.org/10.1038/nature25476
Soykeabkaew, N., Nishino, T., & Peijs, T. (2009). All-cellulose composites of regenerated cellulose fibres by surface selective dissolution. *Composites Part A: Applied Science and Manufacturing, 40*(4), 321–328. https://doi.org/10.1016/j.compositesa.2008.10.021
Starov, V. M., & Velarde, M. G. (2019). *Wetting and Spreading Dynamics*. CRC Press. https://doi.org/10.1201/9780429506246
Tanpichai, S., Boonmahitthisud, A., Soykeabkaew, N., & Ongthip, L. (2022). Review of the recent developments in all-cellulose nanocomposites: Properties and applications. *Carbohydrate Polymers, 286*, Article 119192. https://doi.org/10.1016/j.carbpol.2022.119192
Uusi-Tarkka, E.-K., Levanič, J., Heräjärvi, H., Kadi, N., Skrifvars, M., & Haapala, A. (2022). All-cellulose composite laminates made from wood-based textiles: Effects of process conditions and the addition of TEMPO-oxidized nanocellulose. *Polymers, 14*(19), 3959. https://doi.org/10.3390/polym14193959
Uusi-Tarkka, E.-K., Skrifvars, M., & Haapala, A. (2021). Fabricating sustainable all-cellulose composites. *Applied Sciences, 11*(21), 10069. https://doi.org/10.3390/app112110069
Wenzel, R. N. (1936). Resistance of solid surfaces to wetting by water. *Industrial & Engineering Chemistry, 28*(8), 988–994. https://doi.org/10.1021/ie50320a024
Williams, C., Summerscales, J., & Grove, S. (1996). Resin infusion under flexible tooling (RIFT): A review. *Composites Part A: Applied Science and Manufacturing, 27*(7), 517–524. https://doi.org/10.1016/1359-835X(96)00008-5
Wohlert, M., Benselfelt, T., Wågberg, L., Furó, I., Berglund, L. A., & Wohlert, J. (2022). Cellulose and the role of hydrogen bonds: Not in charge of everything. *Cellulose*, (29), 1–23. https://doi.org/10.1007/s10570-021-04325-4
Yang, J., Dahlström, C., Edlund, H., Lindman, B., & Norgren, M. (2019). pH-responsive cellulose–chitosan nanocomposite films with slow release of chitosan. *Cellulose, 26*(6), 3763–3776. https://doi.org/10.1007/s10570-019-02357-5
Yang, Q., Lue, A., & Zhang, L. (2010). Reinforcement of ramie fibers on regenerated cellulose films. *Composites Science and Technology, 70*(16), 2319–2324. https://doi.org/10.1016/j.compscitech.2010.09.012
Yang, X., & Berglund, L. A. (2018). Water-based approach to high-strength all-cellulose material with optical transparency. *ACS Sustainable Chemistry & Engineering, 6*(1), 501–510. https://doi.org/10.1021/acssuschemeng.7b02755
Ye, D., Yang, P., Lei, X., Zhang, D., Li, L., Chang, C., Sun, P., & Zhang, L. (2018). Robust anisotropic cellulose hydrogels fabricated via strong self-aggregation forces for cardiomyocytes unidirectional growth. *Chemistry of Materials, 30*(15), 5175–5183. https://doi.org/10.1021/acs.chemmater.8b01799